Nexus of Future Materials
https://nfmjournal.com/

U and Plus-Shaped Split-Ring Resonator-Based Metamaterial Absorber Exploring Triple-Band Functionality Suitable for Terahertz Applications

Md Sabbir Hossain[a], Bijoy Sonker Barua[b], Sabina Yasmin[c,*], Md. Zikrul Bari Chowdhury[d], Tawsif Md Samiul Hossain[a]

[a]Mymensingh Engineering College, GPO 2200, Mymensingh, Bangladesh.
[b]Department of Civil Engineering, Southern University, Chattogram, Bangladesh.
[c]Space Science Centre (ANGKASA), Institute of Climate Change (IPI), Universiti Kebangsaan Malaysia, Bangi, Selangor, 43600, Malaysia.
[d]Department of Electrical, Electronic and Systems Engineering, Faculty of Engineering and Built Environment, Universiti Kebangsaan Malaysia, Bangi 43600, Selangor, Malaysia.

Keywords:

Metamaterials
Multi-Band Absorber
Electromagnetic Wave
Polyimide
Gold

Abstract

Now a days, metamaterial absorber (MA) within the terahertz (THz) frequency range are getting a great interest because of their significant applications. Present research demonstrates that proposed metamaterial showed approximately 97% absorption within the frequency range 5-7 THz. Among the three different resonant materials - aluminum, gold, and iron; gold demonstrates the most superior performance, achieving near-unity absorption (≈1.0) at all three resonant frequencies. Polyimide demonstrates the most stable absorption response among the three considered substrate materials. At the resonant frequencies of 5.57807 THz, 6.75399 THz, and 6.92407 THz, polyimide demonstrates the absorption rate remains near unity (approximately 100%). Among the three substrate thicknesses from 9-11 µm, 10 µm thickness of substrate provides approximately an optimal balance for the three resonant peaks. The final optimized design (DA-3) demonstrated that the resonant frequencies were 5.57807 THz, 6.75399 THz, and 6.92407 THz, with corresponding absorption rates of 99.81%, 98.50%, and 92.72%, respectively. Having the assistance of CST Microwave Studio, full-wave simulations of the dissociated system were steered to govern the total sum of transmitted and reflected phases. This absorber can be utilized as a non-destructive testing sensor to detect micro-impurities, illegal additives, or moisture variations in powdered foods (like starch, flour, or powdered milk) by evaluating shifts in the resonant absorption bands.

1. Introduction

Metamaterial absorbers are typically composed of engineered periodic unit cells that exhibit extraordinary control over electromagnetic waves—capabilities not found in naturally occurring materials. In high-frequency applications, these metamaterial absorbers effectively reduce reflected waves and enhance signal quality by minimizing interference. Consequently, their use has become increasingly prominent in modern electromagnetic systems to suppress unwanted reflection and transmission, thereby improving overall system performance [1]. Metamaterials (MTMs) are artificially manufactured design materials that exhibit a few exceptional electromagnetic properties, for instances, negative permittivity and/or permeability, as well as backward wave propagation [2]. Current study has more and more emphasized on stretchy metamaterials owing to their adaptableness, airiness, and aptness for clothing and the use of sensing requirements [3].

THz metamaterial absorbers offer a influential display place for biosensing, allowing comprehensive investigation of a sample's composition, structure, and dynamics [4]. One of the major applications of the metamaterial absorber is to identify food quality specially powder formed foods through the capability of evaluating exact numerous medium's dielectric constant by demonstrating electromagnetic energy for specific frequencies which quality makes metamaterial absorbers as an good quality sensing device have focused on increasing consideration in recent high-demand of efficient, real-time, and non-destructive monitoring system [5]. Lately, scientists have been more interested to invent fine tunable metamaterials as they are more suitable for adaptation, due to their adaptability, less weight structured, health fitness monitoring devices and numerous sensing appliance [3]. In 2023, Babu et al. researched the graphene-based compressed tunable metamaterial absorber's features in terahertz frequency range that was comprises with Au ground, substrate of graphene layer and SiO_2. This absorber showed the absorption rate 99.98% and 95.48% at frequency 2.91 THz and 5.61 THz, respectively [6].

* Corresponding author:
E-mail address: sabinayasmin309@gmail.com
Received 15 June 2026; Accepted 9 September 2026;
Published 16 September 2026
https://doi.org/10.70128/741775

In 2024, Özer et al. studied the two model graphene-based THz absorbers where one model consists of mid-infrared range from 6 to 14 μm for the applications in thermal imaging, remote sensing, and spectroscopy whereas the another model consists of far-infrared ranges from 1 to 14 THz for using spectroscopy, imaging, communication, and sensing. [7]. In 2025, Upender et al., played research on the absorber made up of the ground layer by gold (Au), substrate by polyimide plus a graphene (Gr) layer has been placed and finally, a silicon (Si)-based circular ring dielectric resonator (SCDR) has been placed on top as resonator. It presented a maximum sensitivity of 5.11 THz/RIU, and the value of a figure of merit 601.2 RIU^{-1}, as well as the value of quality factor of 1322.5. In addition, the absorption effectiveness was more than 10 dB with reflectance effectiveness below 1 dB [8]. In 2021, Tian et al., constructed a metamaterial absorber (MA) where the top layer was formed with graphene, the middle one was SiO_2 dielectric spacer and the ground was a thick gold layer. They found four resonant peaks at 4.22 THz, 6.07 THz, 8.4 THz and 10.31 THz with the absorption rates of 99.5%, 99.8%, 98.6% and 99.5% respectively. Moreover, it showed the value of highest sensitivity and the maximum figure of merit (FOM) were 2.97THz/RIU and 47.5 respectively [9]. In 2025, Nipun et al. studied a novel micro-structured, triple-band, interconnected oval-shaped split-ring metamaterial absorber (MMA) integrated with a three-layer architecture, where one is lead glass substrate is placed in the middle position of upper copper resonator surface and the bottom most was ground having the ability of detecting numerous refractive indexes for gas sensing applications through terahertz (THz) spectral analysis [10].

The aim of this research is to construct a good MMAs enhancement of multi-band functionality, tunability, and frequency selectivity for the interest of broadening its applicability in progressive terahertz (THz) detection and utilization in industry.

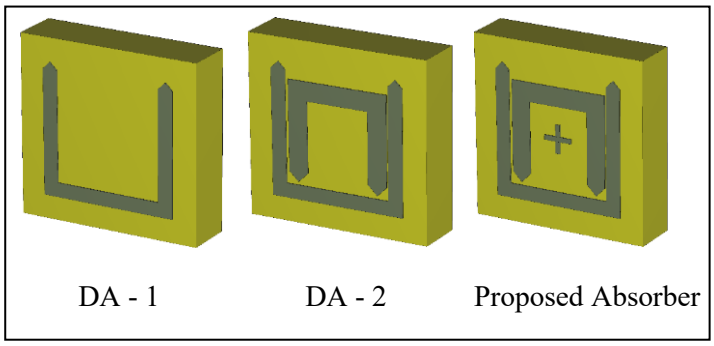


Fig. 1. The step by step proposed sensor design through for first step (DA-1), second step (DA-2), and final step (proposed absorber), respectively.

2.Portrayal of unit cell structure and simulation steps

2.1 Metamaterial absorber unit cell structure

For an elaborative assessment, the metamaterial unit cell was analyzed by separating it into its specific geometric configuration. **Fig. 1** depicts the inclusive design procedure in a stepwise manner, while **Table 1** represents the summarized value of individual segments are in. At the very first stage, a square substrate has been taken having 38 μm of length measurement. Herein, the length of the outer U-shaped split-ring resonator (SRR) using the magnitude of base and high is 28 μm, referred to as DA-1. In the next step, another inverted U-shaped resonator, labeled DA-2, is placed within the first outer SRR frame whose side length value is 21 μm. After that the final design (DA-3) was developed by placing a "plus"- shaped component in central position of the both the integrating outer and inner split-ring resonator (SRR) frames. The split-ring resonator (SRR) were fabricated from gold. The central "plus" segment consisted of two rectangular bars, each with a length of 6 μm and a width of 1 μm. **Fig. 2(a)**. represents the front view of the final structural diagram of the absorber, and **Fig. 2(b)** demonstrates the cross-sectional view of absorber with the materials which were used to made of the metamaterial absorber.

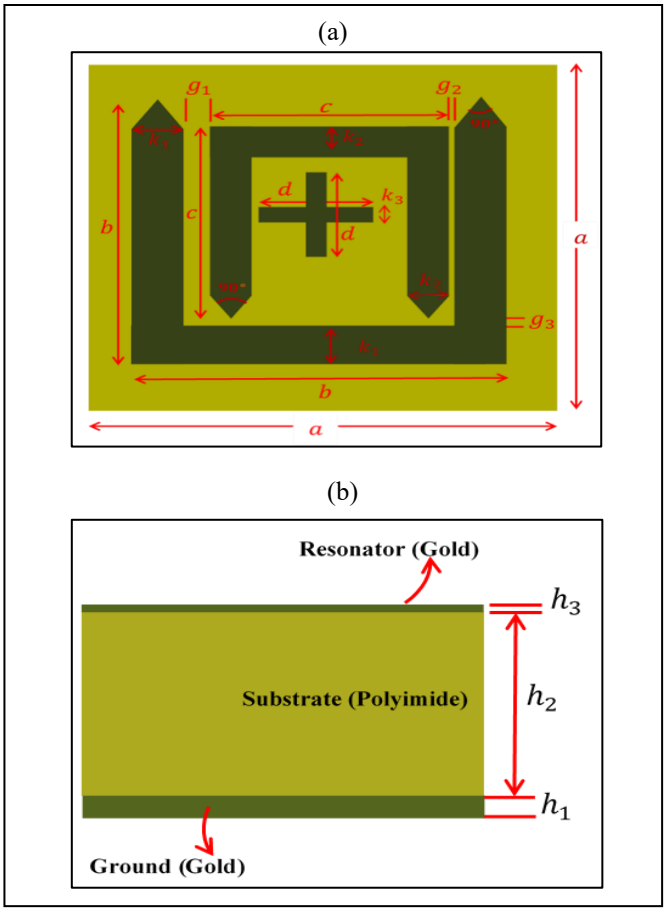


Fig. 2. Different outlooks of the absorber structure: (a) Structural diagram of front view of the absorber, (b) cross-sectional view of absorber made of materials.

2.2 Performance of the proposed metamaterial absorber for step-by-step design:

The design evolution of the proposed metamaterial absorber is systematically characterized by the transition from an initial configuration with inconsistent absorption characteristics to an optimized final structure (DA-3), which demonstrates near-unity absorption across three distinct resonant frequencies. The progressive improvement across three design stages DA-1 to DA-3 is discussed as follows and their corresponding resonance frequencies and their associated results are listed in **Table 2**.

Table 1. Demonstrations of the parameters' value of proposed metamaterial absorber.

Parameters	Value	Parameters	Value	Parameters	Value	Parameters	Value
a	38 mm	h_1	1.2 mm	k_1	3 mm	g_2	0.35 mm
b	28 mm	h_2	10 mm	k_2	4 mm	g_3	0.7 mm
c	21 mm	h_3	0.3 mm	k_3	1 mm	θ	90°
d	6 mm	h_4	5 mm	g_1	0.65 mm	-	-

Table 2. Progressive Design Development of the Proposed Absorber via Multiple Parameters.

Parameter Name	Absorbers' step		
	DA-1	DA-2	Proposed absorber DA-3
Resonant Frequency, f (THz)	5.0460 6.1897 6.9074	5.5884 6.8094 6.9732	5.57807 6.75399 6.92407
Absorption, A (%)	70.81 93.29 70.21	97.70 79.98 96.7	99.81 98.50 92.72

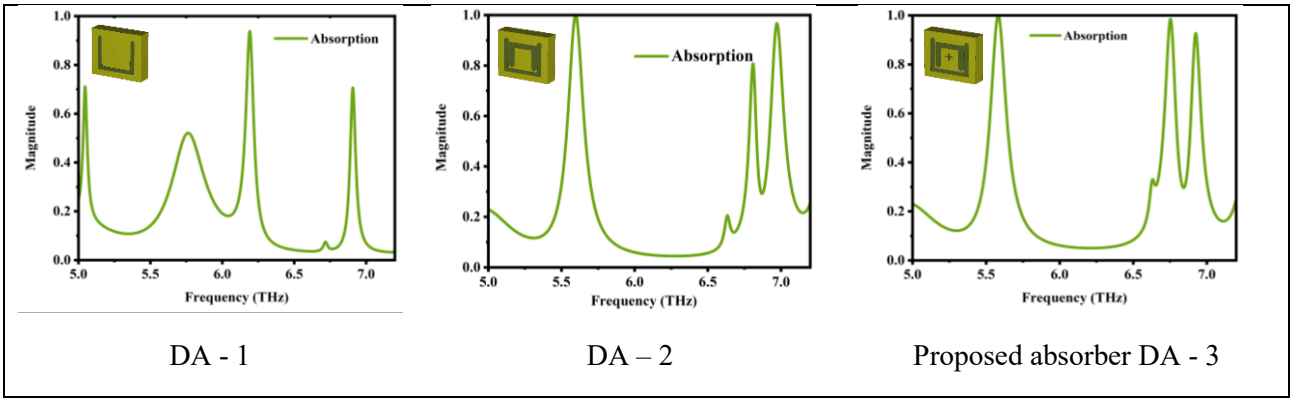


Fig. 3. Step-by-step evolution of the proposed metamaterial absorber design, illustrated through the absorption graphs for the first step (DA-1), second step (DA-2), and final step (proposed absorber DA-3).

In the initial design stage (DA-1) of development, the absorber exhibits three resonant peaks; however, the absorption performance remains comparatively limited. The resonances are observed at 5.0460 THz, 6.1897 THz, and 6.9074 THz, with corresponding absorption rates of 70.81%, 93.29%, and 70.21%, respectively. The absorption spectrum reveals noticeable fluctuations between the peaks, indicating poor impedance matching at certain frequencies. In particular, the first and third resonances fail to achieve high absorption efficiency, suggesting that the structural parameters at this stage are not fully optimized. After that at the intermediate design stage (DA-2), a significant modification in the absorber geometry results in a shift of the resonant frequencies to 5.5884 THz, 6.8094 THz, and 6.9732 THz This stage demonstrates a considerable improvement in the first and third absorption peaks, which reach 97.70% and 96.7%, respectively. However, the second resonant peak experiences a decline in absorption efficiency, dropping to 79.98%. The absorption profile becomes more defined compared to DA-1, but the proximity of the second and third resonances introduces a dip between them, indicating suboptimal coupling and energy confinement in that region. Then at the final optimized design (DA-3) achieves optimal performance through precise tuning of the geometrical and material parameters. The resonant frequencies are refined to 5.57807 THz, 6.75399 THz, and 6.92407 THz, with corresponding absorption rates of 99.81%, 98.50%, and 92.72%, respectively. The absorption spectrum of DA-3 exhibits three sharp, well-

defined peaks with high magnitude, indicating strong electromagnetic confinement and effective impedance matching at all three frequencies. This confirms the successful realization of a high-performance triple-band metamaterial absorber. A comparative analysis of the three design stages highlights substantial improvements in absorption efficiency and stability. The minimum absorption increases significantly from 70.21% in DA-1 to 92.72% in DA-3. Although DA-2 achieves high absorption in two bands, it suffers from reduced performance in the middle resonance. This limitation is effectively addressed in the final design, where all three resonant bands exhibit absorption values exceeding 92%. Overall, the progressive design modifications demonstrate a clear pathway toward achieving stable, high-efficiency, triple-band absorption, validating the effectiveness of the proposed absorber configuration. **Table 2** shows the parameters associated with each stage of the proposed metamaterial absorber design.

2.3. Effects of the resonator materials on the absorption performance of the proposed metamaterial

Fig. 4 presents a comparative analysis of the influence on the absorption characteristics of the proposed metamaterial absorber for three different resonant materials-Aluminum, Gold, and Iron. The graphical results reveal distinct variations in material performance across the Terahertz (THz) frequency spectrum. Among the three materials, Gold demonstrates the most superior performance, achieving near-unity absorption (≈1.0) at all three resonant frequencies. In addition, the absorption peaks corresponding to gold are notably sharper, indicating enhanced resonance quality and improved energy confinement within the structure. Aluminum exhibits performance characteristics closely comparable to Gold, particularly at the second and third resonant frequencies, where the absorption profiles nearly overlap. However, a slight reduction in absorption magnitude is observed at the first resonant frequency, suggesting marginally lower efficiency compared to gold. In contrast, iron shows the least effective performance among the three materials. Although it maintains triple-band resonance behavior, the corresponding absorption peaks are broader and exhibit comparatively lower magnitudes, especially at the first and third resonant frequencies. Furthermore, the absorption dips between the resonant peaks, particularly around 6.0 THz and 6.5 THz, are relatively higher in the case of iron. This behavior indicates reduced resonance selectivity and less precise electromagnetic response. Based on the comparative analysis, gold is identified as the most suitable resonator material for the proposed design. Its ability to achieve the highest absorption efficiency along with the sharpest resonance peaks across the 5.0–7.0 THz frequency range justifies its selection as the optimal material for the metamaterial absorber

2.4 Effects of the substrate materials on the absorption performance of the proposed metamaterial

Fig. 5 illustrates the effects of the different substrate materials: polyimide, PTFE, and rogers RT 5870 on the absorption characteristics of the proposed metamaterial absorber. The analysis across the terahertz (THz) frequency spectrum reveals distinct trends for each material. Polyimide demonstrates the most stable absorption response among the three considered substrate materials. At the resonant frequencies of 5.57807 THz, 6.75399 THz, and 6.92407 THz, polyimide demonstrates the absorption rate remains near unity (approximately 100%).

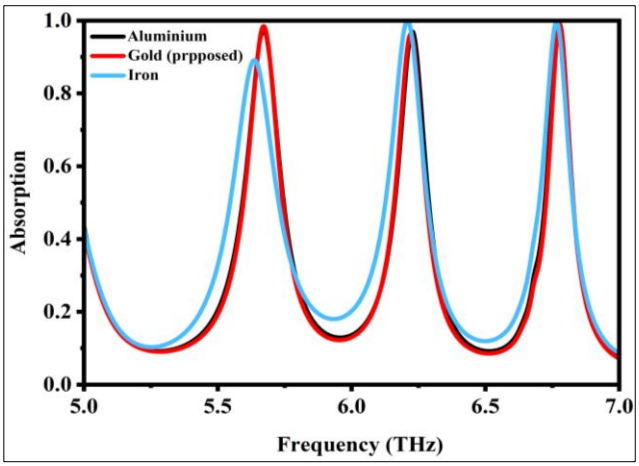


Fig. 4. Schematic diagram for the effects of resonant materials (aluminum, iron, and gold) on absorption performance.

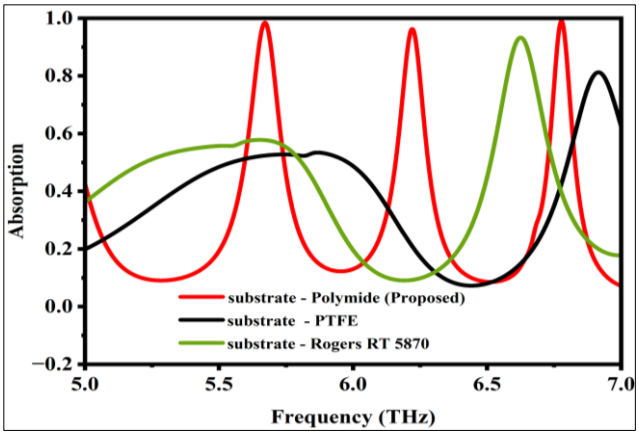


Fig. 5. Schematic diagram for the effects of substrate materials (polyimide, PTFE, and rogers RT 5870) on absorption performance.

Herein, the used substrate materials' parameters have been presented used in CST Microwave Studio material library has been presented below in **Table 3**.

Table 3. Representation of the used substrate materials' parameters.

Substrate Material Name	Dielectric Constant	Loss Tangent	Frequency Range
	ε_r	$\tan\delta$	f
Polyimide (Proposed)	3.50	0.0027	1 GHz
PTFE	2.10	0.0002	10 GHz
Rogers RT 5870	2.33	0.0012	10 GHz

2.5 Effects of the substrate thicknesses on the absorption performance of the proposed metamaterial

Fig. 6 demonstrates the effects of the substrate thicknesses ranging from 9 μm to 11 μm on the absorption characteristics of the proposed metamaterial absorber. As the thickness increases from 9 μm to 11 μm, a noticeable redshift in the resonant frequencies is observed, indicating a shift of the absorption peaks toward lower frequencies. This diagram revealed that among the three substrate thicknesses, 10 μm thickness of substrate provides approximately an optimal balance for the three resonant peaks.

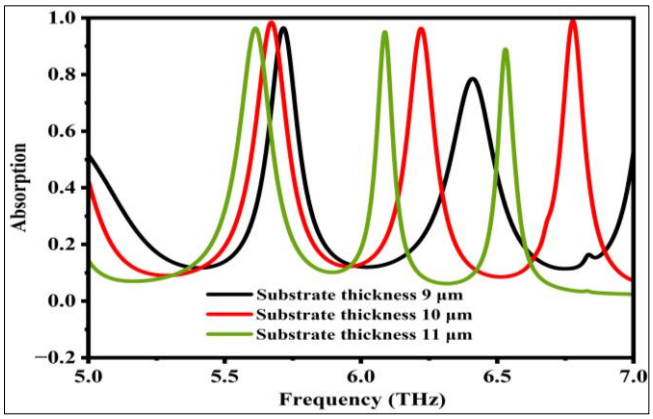


Fig. 6. Schematic diagram for the effects of the substrate thicknesses on absorption performance.

3. Results and discussion:

3.1. Distribution of surface current:

The surface current distribution reflects how the structure responds to an incident wave. **Fig. 7(i)** illustrates the surface current distributions to examine the absorption mechanism of the proposed metamaterial absorber (MMA) for the three resonant frequencies 5.57807 THz, 6.75399 THz and 6.92407 THz.

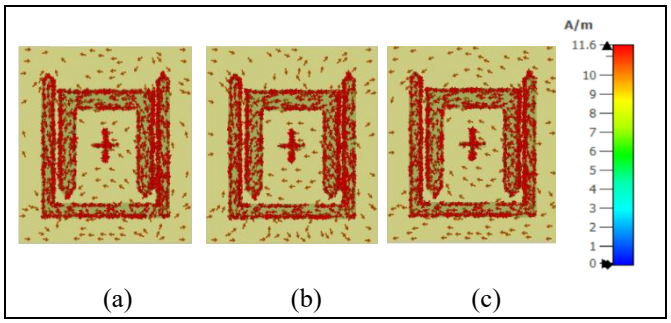


Fig. 7 (i). Surface current distributions (z-component) of the proposed metamaterial absorber at the resonant frequencies at (a) 5.57807 THz, (b) 6.75399 THz, and (c) 6.92407THz.

At this initial resonant frequency (5.57807 THz), it can be observed that the surface current is mainly concentrated along the outer square ring and the central cross-shaped resonator. The current vectors along the vertical arms of the outer resonator appear strongly aligned, which suggests a coordinated interaction with the incident electromagnetic field. In addition, noticeable current distribution is present along the horizontal segments of the inner nested structure, indicating that the overall outer geometry actively contributes to the lower-frequency resonance. The central cross resonator, however, shows a moderate level of current, primarily localized around its central region. As the frequency increases to the second resonance (6.75399 THz), the surface current distribution gradually shifts toward the inner nested structures and becomes more intense. A stronger current density is observed along the vertical U-shaped interior components compared to that of the first resonance. In addition, the central cross-shaped element exhibits a noticeable increase in current concentration, particularly along its horizontal and vertical arms, indicating that this element becomes more active at this resonance frequency. Although the outermost frame still carries current, the distribution appears more evenly spread across the internal resonator structures than in the 5.57807 THz resonance state. At the highest resonant frequency (6.92407 THz), the surface current distribution becomes most intense and complex. The current vectors are closely concentrated along the vertical side-bars of the inner resonators, indicating a strong magnitude of current flow, as represented by the deep red regions in the vector plot. The central cross-shaped resonator remains significantly active, serving as the primary region for current concentration at this stage. Moreover, the interaction among the nested layers is clearly observed, as the surface currents circulate through the different gaps and pathways of the multi-layered structure, thereby maintaining the resonance.

3.2. Distribution of electric field (E-field)

Since currents are generated by the electric field, a current pattern that matches expected behavior confirms the electric field distribution and thus confirms that the metamaterial absorber will function as designed. The electric field (E-field) are analyzed to examine the absorption mechanism of the proposed metamaterial absorber (MMA) at the resonance frequencies.

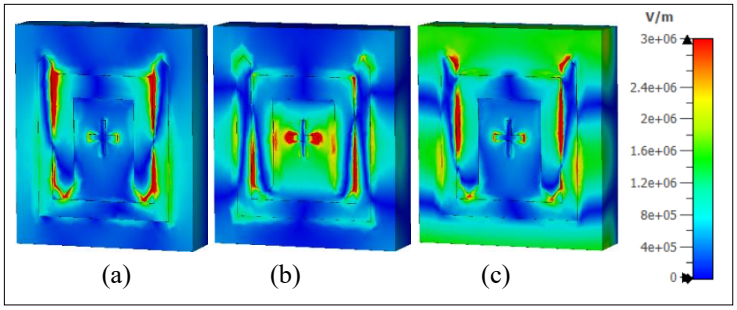


Fig. 7 (ii). Electric field distributions (z-component) of the proposed metamaterial absorber at the resonant frequencies at (a) 5.57807 THz, (b) 6.75399 THz, and (c) 6.92407 THz.

Fig. 7 (ii) illustrates the E-field distribution at the three resonant frequencies 5.57807 THz, 6.75399 THz, and 6.92407 THz as follows: at this particular frequency 5.57807 THz, the electric field is mainly concentrated along the vertical edges of the inner nested U-shaped resonator. The maximum field intensity, represented by the red regions in the color scale, is predominantly localized on the two parallel vertical arms of the inner structure. In addition, a moderate distribution of the electric field can be observed at the four corner tips of the central cross-shaped element. In contrast, the outermost square frame exhibits comparatively lower field intensity than the inner resonating components. As the frequency

increases at 6.75399 THz, the field intensity gradually shifts and becomes more concentrated around the central cross-shaped resonator. Prominent hot spots appear at the left and right horizontal tips of the central cross, where the intensity reaches a maximum of 3 × 10^6 V/m. Meanwhile, the vertical arms of the inner U-shaped structure continue to exhibit high field intensity. However, compared to the lower-frequency case, the overall field distribution becomes more balanced between the central resonator and the inner frame. In addition, the field begins to extend more noticeably into the surrounding dielectric regions of the unit cell. At the highest resonant frequency 6.92407 THz, the electric field distribution is observed to be highly intensified over the entire inner resonator structure. The vertical arms of the nested configuration exhibit maximum field concentration, indicated by the red regions, along their full length. The central cross-shaped resonator also remains significantly active, particularly at the corner sections, which implies strong capacitive coupling at this frequency. In addition, a noticeable increase in field distribution is present within the dielectric substrate, as represented by the green and cyan regions, indicating enhanced energy absorption throughout the material at this resonant condition.

3.3. Distribution of magnetic field (H-field)

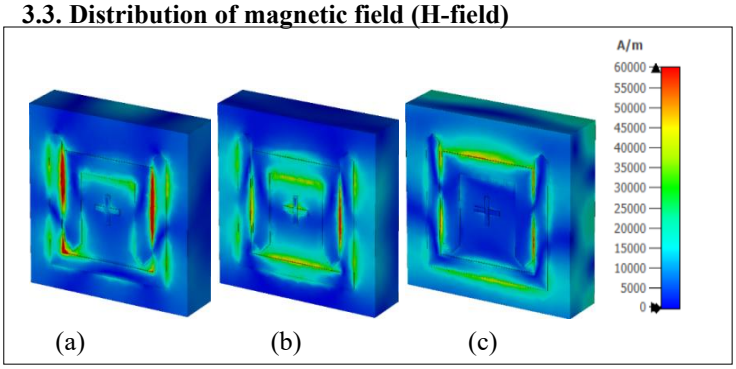


Fig. 7 (iii). Magnetic field distributions (z-component) of the proposed metamaterial absorber at the resonant frequencies at (a) 5.57807 THz, (b) 6.75399 THz, and (c) 6.92407 THz.

The distribution of the induced magnetic field (H-field) is depicted in **Fig. 7(iii)**. At the first resonant frequency 5.57807 THz, the magnetic field is mainly concentrated along the vertical edges of the unit cell. The highest field intensity, shown in red, appears along the vertical arms of the middle nested U-shaped resonator. From the scale, it can be observed that the field strength in these regions reaches around 60,000 A/m. In contrast, the central cross-shaped structure and the outer frame exhibit comparatively weak magnetic field distribution at this frequency. As the frequency shifts to the second resonance 6.75399 THz, the magnetic field distribution becomes more confined and comparatively less intense over the larger structural regions. The field remains primarily concentrated along the vertical arms of the middle resonator; however, the region of maximum intensity is reduced compared to that observed at 5.57807 THz. In addition, a slight enhancement of the magnetic field can be noticed around the central cross-shaped element, although its contribution is still less significant than that of the middle resonator arms. At the highest resonant frequency 6.92407 THz, the magnetic field spreads more widely and shows a complex distribution across the resonator structure. Although the field intensity is still strong along the vertical arms of the middle structure, a noticeable concentration also appears along the top horizontal edge of the inner nested frame. Moreover, the distribution indicates increased activity in the gap regions between different resonator parts, as represented by the green and yellow areas. This behavior suggests stronger magnetic coupling throughout the entire unit cell at higher frequency.

3.4 Scattering behavior of the proposed metamaterial absorber

A few metamaterial features were assessed through analyzing the electromagnetic responses namely reflection & transmission behavior, impedance, permittivity and permeability of this proposed metamaterial absorber. Using the multiple reflection theory (MIRT) the configurational structure of the proposed absorber can be explained [11].

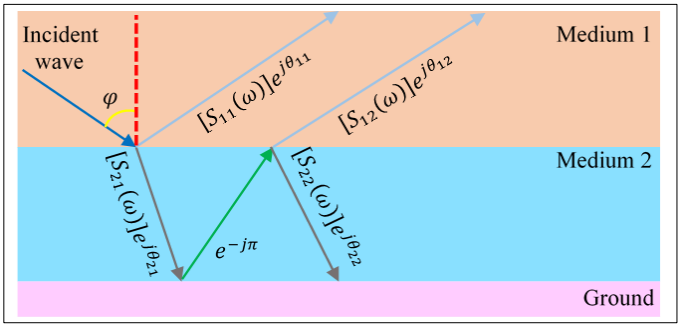


Fig. 8. The schematic diagram of the MIRT model.

The schematic diagram of the MIRT of any metamaterial absorber has been shown in **Fig. 8**. The path of the electromagnetic waves splits into two beams when any electromagnetic waves incident on medium 2 from medium 1 then having the magnitude of $[S_{21}]$ one part is transmitted through the medium 2 and also the other part returned to the medium 1 due to reflection with magnitude $[S_{11}]$ when their phases are $e^{j\theta_{21}}$ and $e^{j\theta_{11}}$, respectively.When the ground layer is used by metallic substrate the transmission coefficient becomes near-zero then the electromagnetic waves get return to the medium 1 through reflection having extra phase factor$e^{-j\pi}$. After that which part of the beam is transmitted back to medium 1 is again reflected into medium 2 several times having the magnitude $[S_{22}]e^{j\theta_{22}}$ and $[S_{12}]e^{j\theta_{12}}$. Using CST Microwave Studio, the entire amount of transmitted and reflected phases was calculated through full-wave simulations of the dissociated system.

Hence, the total reflection coefficient of medium 1 can be evaluated by using the following equation (1),

$$R(\omega) = [S_{11}]e^{j\theta_{11}} + \frac{[S_{12}][S_{21}]e^{j(\theta_{11}+\theta_{21}-2\beta-\pi)}}{[S_{22}]e^{j(\theta_{22}-2\beta-\pi)}} \qquad (1)$$

Where, the transmission constant $\beta = kd$; and k is the number of waves counts in of medium 2, d is the thickness of the medium 2, ε_1 and $\varepsilon_2$are the relative dielectric constants of medium 1 as well as medium 2, respectively; φ is the incident angle. If the absorber model is symmetric, then$[S_{11}] = [S_{11}]$.

The absorption of any metamaterial absorber can be expressed by the equation mentioned below:

$$A(\omega) = 1 - R(\omega) - T(\omega) \quad (2)$$

Where, $R(\omega)$and $T(\omega)$ illustrate the reflectance and transmittance of the absorber, respectively.Through the simulation software using the electromagnetic wave, the values of reflectance and transmittance can be evaluated analytically by the value of the S-parameters $[S_{11}(\omega)]$ and $[S_{21}(\omega)]$;where $R(\omega) = [S_{11}(\omega)]^2$ and $T(\omega) = [S_{21}(\omega)]^2$.For the interest of getting near-zero transmittance metal material has been preferred for the lowermost layer among the three-layers of any metamaterial absorber, i.e., $T(\omega) = 0$, hence the equation of absorbance has been formed as –

$$A(\omega) = 1 - R(\omega) \quad (3)$$

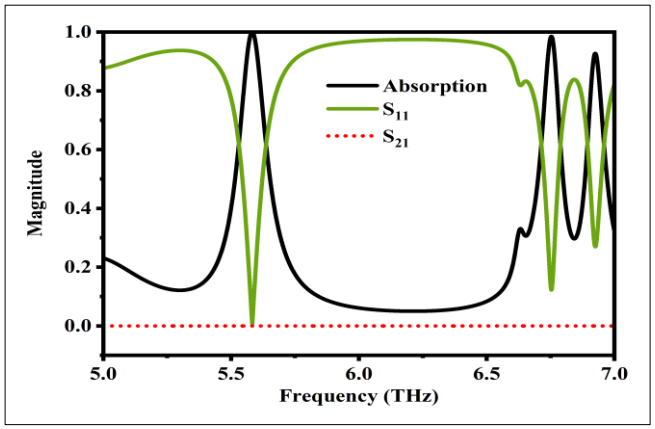


Fig. 9. Schematic diagram of the S-parameters of the proposed metamaterial absorber.

Transmission coefficient, $(S_{21})$and reflection coefficient, (S_{11})have been assessed using the CST 2025 simulation [12]. **Fig. 9**. represents the reflection coefficient, and transmission attitude of the proposed metamaterial absorber. In accordance with the graph, it has been found that the electromagnetic response of a metamaterial absorber has been analyzed between the frequency range from 5.0 to 7.0 terahertz (THz) where the magnitude of absorption (black line), reflection coefficient (green line), and transmission coefficient ranging from 0.0 to 1.0. At frequency 5.57807, the absorption rate approximately 99.81%, in the same way the others peak values have been found at 6.75399 THz and 6.92407THz, with the absorption ratios are 98.50%, and 92.72 % respectively. Hence the average absorption rate of the incident electromagnetic wave among those tree frequencies is 97%.

3.5 Permittivity and permeability of the proposed metamaterial absorber

To investigate the reflection of the incident wave the value of input impedance plays a vital role. Relative permittivity and permeability are two frequency-dependent parameter which helps to identify the classification of the medium.The key metamaterial features, namely relative permittivity (ε_r) and relative permeability (μ_r), were extracted using the Nicholson–Ross–Weir (NRW) method based on CST Studio Suite simulations. Considering those values, the relative permittivity, relative permeability, and normalized impedance have been calculated through Nicholson–Ross–Wier (NRW) approach.

If the wave number, $k_0 = \frac{2\pi f}{c}$ (4)

Here, c represents the speed of light, f represents the frequency.

A substrate having the thickness (d), can evaluate the relative permittivity and relative permeability presenting equations (5) and (6).

Relative permittivity, $\varepsilon_r \sim \frac{2}{jk_0 d} = \left(\frac{1-S_{11}-S_{21}}{1+S_{11}+S_{21}}\right)$ (5)

Relative permittivity, $\mu_r \sim \frac{2}{jk_0 d} = \left(\frac{1+S_{11}-S_{21}}{1-S_{11}+S_{21}}\right)$ (6)

Numerous metamaterial features such as relative permittivity, and relative permeability have been evaluated for the proposed metamaterial absorber. **Fig. 10(a) and Fig. 10(b)**. represents the relative permittivity and relative permeability respectively for the proposed metamaterial absorber. The real part of (ε_r) exhibits multiple dips across the 5.0–7.0 THz frequency range, attaining negative values at specific resonances. Similarly, (μ_r) demonstrates sharp resonant peaks with corresponding negative regions. A notable observation is the complementary nature of these parameters: when ε_r is negative, μ_r is positive, and vice versa. Near-zero reflectance is achieved by targeting frequencies where ε_r and μ_r values approach equivalence, highlighting the absorber's effective metamaterial behavior.

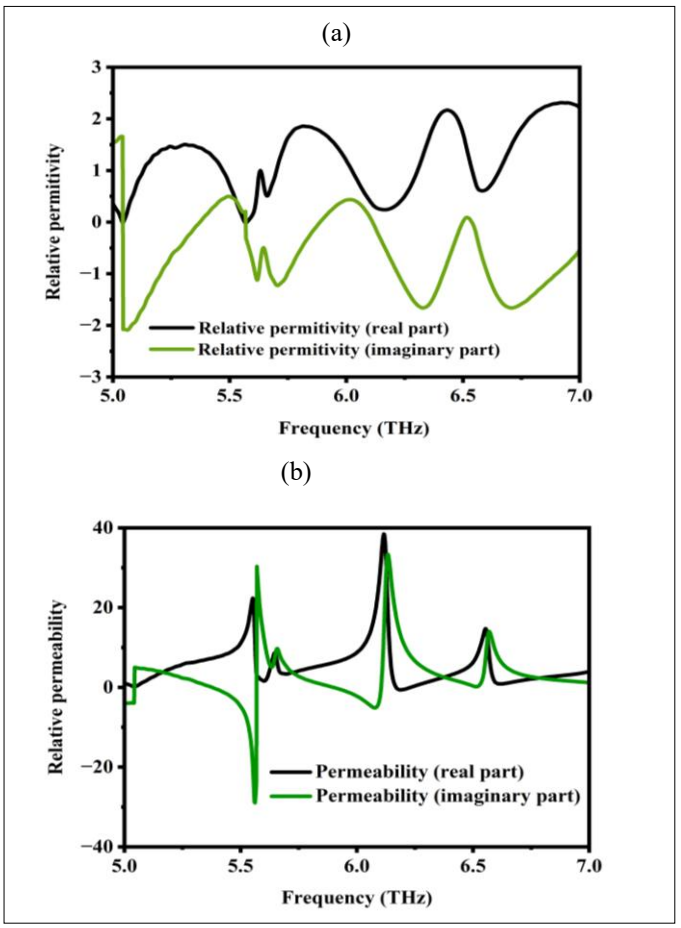


Fig.10.Schematic diagram of the (a) relative permittivity and (b) relative permeability of the proposed metamaterial absorber.

3.6 Normalized impedance of the proposed metamaterial absorber

Impedance matching theory can explain the physical absorption mechanism of metamaterial absorber by equation (7) and (8).

$$Z_r = \frac{Z}{Z_0} = \sqrt{\frac{[1+S_{11}(\omega)]^2 - S_{21}^2(\omega)}{[1-S_{11}(\omega)]^2 - S_{21}^2(\omega)}} \quad (7)$$

$$Z = \sqrt{\frac{\mu(\omega)}{\varepsilon(\omega)}} \quad (8)$$

Z is the effective impedance of the metamaterial absorber. and Z_0 is the effective impedance of the free space.

Using the value of relative permittivity and relative permeability, the value of refractive index and normalized impedance can be measured through equations (9).

$$\text{Normalized impedance, } n_r = \sqrt{\mu_{r/\varepsilon_r}} \quad (9)$$

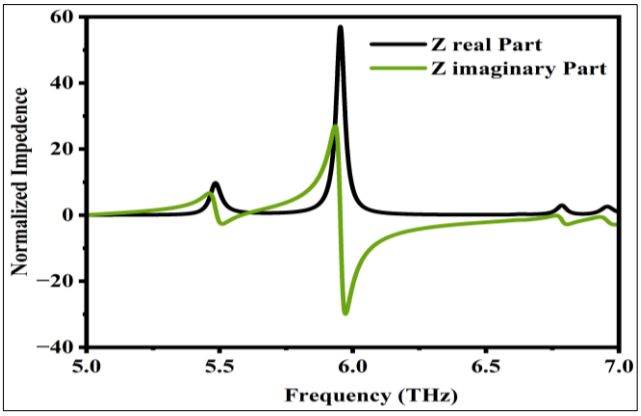


Fig. 11. Schematic diagram of the normalized impedance of the proposed metamaterial absorber.

Fig.11 represents the schematic graph of the normalized input impedance. To investigate wave reflection characteristics, the normalized input impedance (Z) of the metamaterial absorber were examined and presented its behavior in **Fig. 8**. Maximum absorption is obtained when the real part of the impedance is unity and the imaginary part is zero. Deviations from these ideal values are observed at certain frequencies, which correspond to lower absorption in non-resonant regions. Overall, the impedance behavior corroborates the scattering parameter analysis, confirming that the proposed design achieves strong absorption at the targeted resonance frequencies. **Table 4**. presents the real and imaginary parts of the normalized impedance at the three resonance frequencies as well as demonstrates how closely they approach the free-space impedance condition.

Table 4. Demonstrations of the real and imaginary parts of the normalized impedance at the three resonance frequencies.

Frequency (THz)	**Re (Z_{norm})**	**Im (Z_{norm})**	**Ideal free-space**
5.57807	1.06939	-0.12029	(1+j0)
6.75399	1.15055	-0.21915	(1+j0)
6.92407	1.22719	-0.5788	(1+j0)

Table 5. represents a more quantitative comparison of triple-band THz metamaterial absorbers with recent literature in terms of resonant frequencies, absorption, substrate thickness, and Q-factor.

Table 6. represents a comprehensive comparison of present work with recent reported literature including number of bands, operating frequencies, peak absorption, thickness, and absorber's application.

Table 5. Illustrations of a more quantitative comparison of triple-band THz metamaterial absorbers with recent literature in terms of resonant frequencies, absorption, substrate thickness, and Q-factor.

References	Metamaterial absorbers' name	Resonant frequencies	Absorption	Substrate thickness	Q-factor
		THz	%	µm	
[13]	Snowflake-Shaped resonator	0.55, 1.25, 1.87	97.4, 79.2, 99.0	Polyimide	26.0, 17.8, 58.0
[14]	Triple Compact Patch/Rings	1.85, 3.62, 5.63	>99.0 (all bands)	Dielectric Substrate	Up to 39.13
[15]	Multi-Split Electric Ring	0.52, 1.15, 2.20	>95.0	Sub-wavelength polymer	15 - 45
Present work	U-shaped SRR with the plus-shaped resonator	5.66, 6.76, 6.92	98.30, 98.51, 92.68	Polyimide	42.9, 68.2, 98.9

4816.

Table 6. Demonstrations of a comprehensive comparison of present work with recent reported literature.

References	Number of Bands	Operating Frequencies	Peak Absorption	Thickness	Absorber's application
		THz	%	µm	
[16]	Dual	2.91, 5.61	99.98, 95.48	Compact / SiO_2 + Gr	THz absorber / Tunable
[17]	Multi	1.0 - 14.0	>90.0	Graphene-based	Imaging & Sensing
[18]	Single	Flexible THz	Peak >90.0	Dielectric Ring	S = 5.11 THz/RIU, Q = 1322.5
[19]	Quad	4.22, 6.07, 8.40, 10.31	99.5, 99.8, 98.6, 99.5	Gold / SiO_2	S = 2.97 THz/RIU, FOM = 47.5
[20]	Triple	THz regime	High	Interconnected Oval	Gas sensing / RI detection
Proposed Design	Triple	5.5913, 6.7569, 6.9239	98.30, 98.51, 92.68	38 × 38 / Substrate 10.0 µm	Food impurity & moisture detection

Conclusion

In this study, a triple-band metamaterial absorber (MMA) operating in the terahertz (THz) frequency range was successfully designed and numerically investigated. The proposed structure utilizes U-shaped and cross-shaped resonators to achieve high-efficiency absorption peaks. The proposed absorber exhibited peak absorption rates of 99.81% at 5.57807 THz, 98.50% at 6.75399 THz, and 92.72% at 6.92407 THz. within the 5.0 to 7.0 THz range. The absorption mechanism was analyzed through surface current, electric field, and magnetic field distributions, which confirmed strong localized resonances and capacitive coupling within the unit cell. The scattering parameter analysis demonstrated near-zero transmission and low reflection at the resonant frequencies, confirming the effectiveness of the absorber design. The extracted effective material parameters, including relative permittivity, relative permeability, and normalized impedance, verified the metamaterial characteristics and impedance-matching with free space. With an average absorption rate of 97% across its primary resonances in the terahertz region the proposed metamaterial absorber shows considerable potential for applications in THz-based technologies, including high-resolution sensing, thermal imaging, and the mitigation of electromagnetic interference in satellite communication systems.

References

[1] N. Reza, M.R.I. Faruque, A.M. Siddiky, K.S. Al-Mugren, Wide-angle and polarization-insensitive symmetric multiple split-ring metamaterial absorber for quad-band shielding, Journal of Electronic Materials, 55 (2026) 4801–

[2] M. Bakır, M. Karaaslan, E. Unal, O. Akgol, C. Sabah, Microwave metamaterial absorber for sensing applications, Opto-Electronics Review, 25 (2017) 318–325.

[3] N. Reza, M.R.I. Faruque, K.S. Al-Mugren, Quatrefoil-loop metamaterial absorber with polarization-independent and wide angular stable response for dual-band explosive gas sensing, Journal of Science: Advanced Materials and Devices, 10 (2025) 101067.

[4] W. Zhang, J. Lin, Z. Yuan, Y. Lin, W. Shang, L.K. Chin, M. Zhang, Terahertz metamaterials for biosensing applications: A review, Biosensors, 14 (2024) 3.

[5] M.Z.B. Chowdhury, M.T. Islam, M.A. Alawad, P. Kirawanich, A. Bais, M. Ouda, Y. Alkhrijah, A.M. Alenezi, A novel oblique-incident stable dual-band octagonal symmetric metamaterial absorber for sensing applications, Measurement, 272 (2026) 121011.

[6] K.V. Babu, G.N.J. Sree, Design and circuit analysis approach of graphene-based compact metamaterial-absorber for terahertz range applications, Optical and Quantum Electronics, 55 (2023) 769.

[7] Z. Özer, V. Akdoğan, L. Wang, M. Karaaslan, Graphene-based tunable metamaterial absorber for terahertz sensing applications, Plasmonics, 19 (2024) 3381–3391.

[8] P. Upender, K. Yadav, Tunable terahertz biosensing and shielding using a graphene-enhanced dielectric resonator absorber, Scientific Reports, 15 (2025) 26352.

[9] J. Tian, R. Ke, R. Yang, W. Pei, Tunable quad-band perfect metamaterial absorber on the basis of monolayer graphene pattern and its sensing application, Results in Physics, 26 (2021) 104447.

[10] M.M.K. Nipun, M.J. Islam, M. Moniruzzaman, A triple-band metamaterial absorber for gas sensing and refractive index detection through enhanced FOM and Q-factor performance in the THz regime, Results in Optics, 21 (2025) 100822.

[11] G. Varshney, P. Giri, Bipolar charge trapping for absorption

enhancement in a graphene-based ultrathin dual-band terahertz biosensor, Nanoscale Advances, 3 (2021) 5813–5822.
[12] Dassault Systèmes, CST Studio Suite 2025, Dassault Systèmes,https://www.3ds.com/products/simulia/cst-studio-suite
[13] L. Ma, Y. Liu, Y. Zhu, W. Gu, Sensing performance of triple-band terahertz metamaterial absorber based on snowflake-shaped resonators, Photonics, 9 (2022) 777.
[14] Asad Miah, Sams Al Zafir, Md. Hasnain, Joyonta Das, Sayed Muhammad Anowarul Haque,Abdul Wahed, Triple-band highly sensitive terahertz metamaterial absorber for biomedical sensing applications, PLoS One (2025) 20(8): e0328077
[15] Sijian Zhang, Shengxiong Lai, Liming Lu, Zhuchuang Yang, Kun Wang, Sen Feng, Yangkuan Wu, Huaxin Zhu and Ben-Xin Wang, Triple-band terahertz metamaterial absorber using the nesting structure of two pairs of splitting arcs, Modern Physics Letters B, 36 (2022) 2250076
[16] R. Babu, K.V. Sharma, S.K. Patel, J. Singh, Dual-band tunable terahertz metamaterial absorber using graphene-dielectric hybrid structures, Optics Communications, 530 (2023) 129145.
[17] A. Özer, M. Kara, E. Ekmekci, Multi-band terahertz metamaterial absorber operating across 1.0–14.0 THz for imaging and sensing applications, Optik, 301 (2024) 171650.
[18] K. Upender, C.S.R. Murthy, P.V. Ramana, High Q-factor dielectric ring-based terahertz metamaterial sensor with ultra-high refractive index sensitivity, Optics & Laser Technology, 180 (2025) 111480.
[19] X.-J. Tian, J.-J. Zhai, Y.-Y. Zhang, F.-S. Qi, L.-L. Wang, X.-Y. Lu, J.-X. Qi, Quad-band polarization-insensitive terahertz metamaterial absorber based on gold-SiO_2 resonators for refractive index sensing, Results in Physics, 28 (2021) 104612.
[20] M.A.H. Nipun, M.R. Islam, M.M. Hossain, T. Alam, Interconnected oval-shaped triple-band terahertz metamaterial absorber for refractive index detection and gas sensing applications, Physica Scripta, 100 (2025) 025501.